Ocean Sci. Discuss., 12, 897–924, 2015
www.ocean-sci-discuss.net/12/897/2015/
doi:10.5194/osd-12-897-2015
© Author(s) 2015. CC Attribution 3.0 License.

Ocean Science
Discussions
Open Access

This discussion paper is/has been under review for the journal Ocean Science (OS).
Please refer to the corresponding final paper in OS if available.

Shifting momentum balance and frictional adjustment observed over the inner-shelf during a storm

M. Grifoll[1,2], **A. Aretxabaleta**[3], **J. L. Pelegrí**[4], **and M. Espino**[1,2]

[1]Maritime Engineering Laboratory, Technical University of Catalonia, Barcelona, Spain
[2]International Centre of Coastal Resources Research, Barcelona, Spain
[3]US Geological Survey, Woods Hole, USA
[4]Department of Physical and Technological Oceanography, Marine Science Institute, Barcelona, Spain

Received: 27 April 2015 – Accepted: 4 May 2015 – Published: 27 May 2015

Correspondence to: M. Grifoll (manel.grifoll@upc.edu)

Published by Copernicus Publications on behalf of the European Geosciences Union.

Abstract

We investigate the rapidly changing equilibrium between the momentum sources and sinks during the passage of a two-peak storm over the Catalan inner-shelf (NW Mediterranean Sea). Velocity measurements at 24 m water depth are taken as representative of the inner shelf, and the cross-shelf variability is explored with additional measurements at 50 m water depth. At 24 m, as the storm-related wind stress accelerated the flow, velocity increased throughout the water column, resulting in bottom stress starting to become important. The sea level also responded, with the pressure gradient force opposing the wind stress. In particular, during the second wind pulse, there were rapid oscillations in the acceleration and advective terms, apparently reflecting the incapacity of the bottom stress to dissipate the high kinetic energy of the system. The Coriolis and wave induced terms (via radiation stresses) were less important in the momentum balance. The frictional adjustment time scale was around 10 h, consistent with the e-folding time obtained from bottom drag parameterizations. Estimates of the frictional time and Ekman depth confirm the prevailing frictional response at 24 m. The momentum evolution in deeper parts of the shelf (50 m) showed an increase in the Coriolis force at the expense of the frictional term, typical in the transition from the inner to the mid-shelf.

1 Introduction

The inner-shelf, encompassing depths ranging from a few to tens of meters, is dynamically defined as a region that lies between the surf zone (where waves break and the momentum balance is dominated by wave-induced terms) and the middle shelf (where the along-shelf circulation is usually in geostrophic balance) (Lentz and Fewings, 2012). The water circulation over the inner-shelf has been studied through the analysis of the momentum balance in different regions, but usually focused on conditions averaged

OSD
12, 897–924, 2015

over periods longer than one week (Lee et al., 1984; Lentz and Winant, 1986; Lentz et al., 1999; Maza et al., 2006; Fewings and Lentz, 2010; Grifoll et al., 2012, 2013).

Energetic wind events, such as storms, modify the typical pattern of water circulation over the continental shelf. The proximity of the coastline and the relevance of bottom friction prevent the generation of inertial fluctuations, which often prevail in the mid and outer shelf following wind pulses (Salat et al., 1992; Shearman et al., 2005). Additionally, during the passage of storms, the intense wind, and in some cases the associated cooling, affects a large fraction of the water column. The frictional adjustment time, proportional to water depth and inversely proportional to wind stress, is largely reduced nearshore during such energetic events. As a consequence, the magnitude, phase and relative importance of the dominant terms in the momentum balance is modified. For instance, during the passage of the tropical storm Floyd in the US east coast, Kohut et al. (2006) found the prevalent terms that the size of the momentum terms increased during the peak of the storm. They highlighted the rise in wind stress and the associated pressure gradient, with changes in sign between the storm and the subsequent relaxation period. Lee et al. (1984) found observational evidence on the sea-level slope opposing the wind stress in order to establish a frictional equilibrium that differed from the average conditions. A seasonal study of the Catalan Shelf (Grifoll et al., 2013) has suggested that the occurrence of one single intense event can dominate the monthly averaged momentum balance with water piling against the coast as a response to the enhanced wind stress; to balance the surface forcing, the bottom stress term was also increased.

In this paper, we investigate the mechanisms causing the shifting momentum balance on short-time scales during a storm. The analysis is based on a set of observations from the Catalan inner-shelf (offshore the city of Barcelona; NW Mediterranean Sea; Fig. 1). The analysis characterizes the evolution of the different momentum terms and examines the response time scales for the principal forcing mechanisms. The prevalent terms at two different depths (24 and 50 m, where data is available) are examined. We take advantage of our setting in a micro-tidal environment to investigate

OSD
12, 897–924, 2015

a temporal scale (from hours to few days) usually not considered in the literature, where the time series are often low-pass filtered to remove the short-term fluctuations (e.g. tidal flow).

2 Site location and data

The Catalan shelf is micro-tidal, with tidal amplitudes of the order of tens of cm. The wind and heat flux regimes exhibit a seasonal cycle associated with the Mediterranean climate and the periodicity of meteorological events in the region. Wind intensity usually has a minimum during warm summer and is more energetic during fall, winter and spring. During these seasons, regional storms are predominantly associated with north and northeast winds alternating with northwesterly wind pulses (land winds). Grifoll et al. (2013) analyzed the resulting seasonal circulation pattern over the inner-shelf through a combination of numerical and observational techniques. The flow is prevalent in the along-shelf direction year-round, which is consistent with the coastal constraint and the shallowness of the area. The monthly averaged along-shelf momentum balance was between wind stress and pressure gradient with bottom stress being a second order term. In the present study, we focus on a subset of the data analyzed by Grifoll et al. (2012) that includes an energetic event lasting a few days.

The bulk of the measurements correspond to a field experiment conducted over the Catalan inner-shelf in the framework of the FIELD_AC project. The data set consisted of velocity time series from three Acoustic Doppler Current Profiler (ADCP) deployments (A1 [AWAC], A2 [AWAC] and A3 [RDI], Fig. 1). The ADCP bin size was 1 m. The along-shore distance between A1 and A2 was 4 km. A1 and A2 were deployed less than 1 km from the coast (24 m bottom depth) while A3 was 2 km away from the coast (50 m bottom depth). Wave data were recorded through a directional wave buoy [Datawell DWR-G7] moored in A3. Wind data were collected using a mast located at a Coastal Station Observatory (CSO; www.pontdelpetroli.org; see Fig. 1).

OSD
12, 897–924, 2015

3 Results

3.1 Event description

The water currents during the entire field campaign were analyzed in a previous study (Grifoll et al., 2012), highlighting the prevalence of the along-shelf direction and the high correlation between the velocities measured at A1, A2 and A3. For this reason, we focus on the A2 observations, considered to be representative of the dynamics in the inner-shelf, and use A1 and A3 to support the momentum term estimates. The investigation of the cross-shelf variability in the along-shelf momentum equation also uses A3 (50 m).

For the current analysis, we focus on the 12–15 March 2011 period, which included the passing of a NE storm with maximum wind intensities of $13\,m\,s^{-1}$. The storm was characterized by two energetic northeasterly wind peaks of similar magnitude (12 March 05:00 UTC and 14 March 15:00 UTC). A relatively calm period in between the peaks lasted 22 h (Fig. 2a; see reference system in Fig. 1) with a slight reverse in wind direction. The storm finished on 15 March when the wind intensity decreased to zero.

The along-shelf velocity in the water column (Fig. 2b) was characterized by a prevalent southwestward flow. The velocity exhibited large vertical shear with near-surface velocities being four times stronger than the near-bottom flow. The cross-shelf flow (Fig. 2c) was less intense than the along-shelf flow and exhibited a complex vertical structure. During the calm day (13 March 00:00–22:00 UTC), the wind changed direction slightly, towards the northeast (peaking at 13 March 15:00 UTC), but the along-shelf currents maintained a similar magnitude and structure than the day before. Meanwhile, the cross-shelf flow was weakly onshore. The second wind peak (14 March 15:00 UTC) was characterized by an intensification of the southeastward flow, while the cross-shelf flow was also enhanced. During the second peak (14 March), the onshore surface flow was compensated by a return flow near the bottom. During the last day of the storm (15 March), the surface wind stress decreased gradually from 0.2 Pa to zero

OSD
12, 897–924, 2015

(15 March 23:00 UTC). The along-shelf flow remained towards the southeast throughout the water column, and the cross-shelf flow was offshore in the sub-surface layers balanced by onshore currents near bottom.

The depth-averaged along-shelf velocities were much larger than the depth-averaged cross-shelf velocities during the two wind peaks (Fig. 2d) consistent with the strong polarization of the flow due to the coastal constraint. During the first day of the storm (12 March), the depth-averaged current in the along-shelf direction (Fig. 2d) was toward the southwest with a maximum peak during 12 March 07:00 UTC. The detided sea level (Fig. 2e) increased during both wind peaks and slowly decreased after the wind peak. After the storm, the sea level increased as a result of water being piled up against the coast due to the northeasterly wind. The wave conditions measured at A3 were characterized by two significant wave height peaks (Fig. 3f) from the E–SE direction with a wave period of 8 s.

3.2 Momentum balance in the inner-shelf

Assuming hydrostatic balance, small sea level variations compared with the total water depth, and neglecting the baroclinic terms (estimated as small in Grifoll et al., 2012 and Grifoll et al., 2013), the depth-averaged along-shelf momentum balance equation can be written as:

$$\underbrace{\frac{\partial \overline{v}}{\partial t}}_{\text{ACCE}} + \underbrace{\frac{\partial \overline{v^2}}{\partial y} + \frac{\partial \overline{uv}}{\partial x}}_{\text{ADVEC}} + \underbrace{f\overline{u}}_{\text{COR}} = \underbrace{-g\frac{\partial \eta}{\partial y}}_{\text{PRS-GRAD}} + \underbrace{\frac{\tau_{ys}}{\rho H}}_{\text{W-STR}} - \underbrace{\frac{\tau_{yb}}{\rho H}}_{\text{B-STR}} - \underbrace{\frac{1}{\rho H}\left(\frac{\partial S_{yy}}{\partial y} + \frac{\partial S_{xy}}{\partial x}\right)}_{\text{RAD-STR}} \quad (1)$$

where $(\overline{u}, \overline{v})$ are the cross- (x) and along-shelf (y) depth-averaged components of velocity, H is the water depth, f is the Coriolis parameter ($f = 9.6 \times 10^{-5}\,\mathrm{s}^{-1}$), ρ is the water density ($1025\,\mathrm{kg\,m}^{-3}$), η is the sea level associated with the barotropic component of the flow, τ_{ys} is the wind stress, τ_{yb} is the bottom stress and S_{yy}, S_{xy} represent the wave induced mass fluxes estimated via radiation stresses (Longuet-Higgins and

OSD
12, 897–924, 2015

Stewart, 1964). The data used for estimating the momentum terms have been low-pass filtered with a $1/12\,h^{-1}$ cut-off frequency to avoid very short-time scale fluctuations. This choice of filter window is consistent with the velocity spectra that showed limited energy in frequencies higher than inertial (Grifoll et al., 2012).

The along-shelf acceleration term at A2 (ACCE in Eq. 1) is estimated from the observations using centered-finite differences with the velocity recorded at A2 (Fig. 3a). A negative peak is observed in the acceleration time serie during the first wind peak. After the wind direction reversal, the acceleration term oscillates indicating a readjustment of the momentum balance (i.e. a relaxation period that lead to the pre-storm conditions).

The non-linear or advection term (ADVEC in Eq. 1) is estimated by finite differentiation between the adjacent ADCP measurements (Kirincich and Bart, 2009). The size of this term is smaller during the first peak of the storm. After the peak, the ADVEC term oscillated in a manner similar to the acceleration term (Fig. 3b).

The Coriolis term (COR in Eq. 1), computed from depth-averaged cross-shelf velocities at A2, follows a complex pattern during the storm (Fig. 3c). Although the surface and sub-surface cross-shelf flows can be relatively important through the water column (Fig. 2c), the depth-averaged cross-shelf flow is much smaller than the along-shelf velocities (Fig. 2d). The size of this term is four times smaller than the acceleration term.

The along-shelf wind stress term (W-STR, Fig. 3d) is calculated using a neutral drag law (Large and Pond, 1981) from winds measured at the nearby meteorological station (Fig. 1). There is a good correspondence between wind stress and along-shelf velocity (Fig. 1a and d). The maximum (negative) acceleration, however, occurs a few hours before the maximum winds (12 March 05:00 UTC and 12 March 07:00 UTC). After the first wind peak the acceleration decreases rapidly and changes sign, becoming small but positive during the remaining of the wind pulse; after the second wind peak, the acceleration displays three rapid oscillations with a period of about 12 h (Fig. 3a).

No direct estimate of the along-shelf pressure gradient (PRS-GRAD in Eq. 1) can be obtained from the data. The ADCP recorded the pressure in the water column but

OSD
12, 897–924, 2015

the distances between ADCPs are not sufficient to capture the along-shelf sea level variability, as the signal-to-noise ratio was not satisfactory. Hickey (1984) pointed out that, for spatial scales of the same order of magnitude as the external Rossby Radius (about 100 km in the Catalan Sea), the expected sea level gradient would be of only a few centimeters. In our case, the sea level variations recorded by the pair of pressure sensors in A1 and A2 (separated by only a few kilometers) were of the same order as the accuracy of the devices (order millimeters). As an alternative approximation, the pressure gradient force is computed using data from a sea level gauge located in the harbor of Blanes (approximately 64 km to the north; Fig. 1) and the ADCP pressure sensor at A2. The resulting pressure gradient force ($-g\frac{\partial n}{\partial y}$) obtained from the observations (PGFO term) represents predominantly remote sea-level effects (Fig. 3e).

The bottom stress (B-STR, in Eq. 1) is estimated using a linear drag law (Lentz and Winant, 1986):

$$\tau_{ys} = \rho r v_b, \tag{2}$$

where r is the linear drag coefficient, ρ is density and v_b is the near-bottom velocity (measured at about 1 m from the sea bottom). The estimation of the drag coefficient depends on the water depth and the along-shelf velocity; significant fluctuations in the value of r have been found to occur as the prevalent momentum terms change (Lentz et al., 1999). Typical values for water depths of a few tens of meters are between 10^{-3} and $10^{-4}\,\mathrm{m\,s^{-1}}$ (e.g. Winant and Beardsley, 1979). In our analysis, the drag coefficient was estimated using the momentum balance evolution, which is explained in the following paragraph.

We approximate the along-shelf pressure gradient force term as the residual from the momentum balance equation when calculated from the wind stress, advection, bottom stress, acceleration and Coriolis terms and define the pressure gradient force obtained from the Residual (PGFR) as:

$$\mathrm{PGFR} = \frac{\partial \overline{v}}{\partial t} + \frac{\partial \overline{v^2}}{\partial y} + \frac{\partial \overline{uv}}{\partial x} + f\overline{u} - \frac{\tau_{ys}}{\rho H} + \frac{\tau_{yb}}{\rho H} + \frac{1}{\rho H}\left(\frac{\partial S_{yy}}{\partial y} + \frac{\partial S_{xy}}{\partial x}\right). \tag{3}$$

OSD
12, 897–924, 2015

Maza et al. (2006) used a similar approach to compute the pressure gradient force when sea level gradient was not available from observations. In our case, the value of r is estimated iteratively until the maximum PGFR matched the maximum PGFO during the first peak of the storm. This strategy resulted in a value of r which is based on the observations and consistent with the evolution of the momentum balance. The resulting value is $8.5 \times 10^{-4}\,\mathrm{m\,s^{-1}}$, comparable to values computed from observations at similar depths (Winant and Beardsley, 1979).

The bottom stress (B-STR) and pressure gradient from residual (PGFR) terms are shown in Fig. 3f and g, respectively. Both the observed and residual pressure-gradient time series (PGFO and PGFR) reproduce the force direction of the sea-level slope during the wind stress peaks (Fig. 3d). The PGFR includes a contribution caused by a direct response to the local wind forcing (for instance during 13 March), which is not immediately obvious in PGFO. During the wind peaks, the positive pressure gradient force partially counterbalanced the wind stress in a manner consistent with other observational studies (Lee et al., 1984; Lentz, 1994; Fewings and Lentz, 2010). In the analysis of the momentum balance evolution, we use PGFR rather than PGFO simply because, even though PGFR exhibited large uncertainty, it is consistent with the estimates for the other momentum terms.

The wave induced mass fluxes (RAD-STR in Eq. 1) are estimated as follows:

$$S_{xy} = E\frac{c_g}{c}\sin(\phi)\cos(\phi), \tag{4}$$

$$S_{yy} = E\left[\frac{c_g}{c}(1+\sin^2\phi) - \frac{1}{2}\right], \tag{5}$$

where the wave energy is computed as $E = \rho_0 g H_{sig}^2/16$, with H_{sig} as the significant wave height, ϕ the wave direction of propagation, and c_g and c respectively as the (linear theory) group and phase velocity at the peak wave frequency. The numerical model SWAN (Booij et al., 1999) was implemented and calibrated (Grifoll et al., 2014) in a 50 m-cell domain, which covered the area of interest (Fig. 1). Radiation stress

OSD
12, 897–924, 2015

gradients are then estimated from two adjacent numerical cells in the proximity of A2 that considered the propagation of wave conditions measured at A3. Both radiation stresses (Fig. 3h) have maximum values during the peaks in significant wave height (about 2.5 m).

3.3 Momentum balance near the mid-shelf

The cross-shelf variability of the along-shelf momentum is estimated by comparing the inner-shelf results with the momentum terms at 50 m water depth. The terms that may be estimated from the velocities observed at A3 are surface and bottom friction, acceleration, and Coriolis force (Fig. 4). The surface stress term is estimated with the local wind measured at CSO, scaled with the corresponding water depth. The non-linear terms are not estimated due to the lack of additional measurements at 50 m, necessary for estimating the along-shelf gradient. Thus, the pressure gradient from the residual is not estimated according to Eq. (3), as not all terms in the right-hand-side were available. Alternatively, we estimate the pressure gradient as a residual (assuming small non-linear effects) considering acceleration, Coriolis and frictional terms (wind and bottom friction), which lead to ($\mathrm{PGFR_{ACCE+COR+FRIC}}$):

$$\mathrm{PGFR_{ACCE+COR+FRIC}} = \frac{\partial \overline{v}}{\partial t} + f\overline{u} - \frac{\tau_{ys}}{\rho H} + \frac{\tau_{yb}}{\rho H}. \quad (6)$$

The bottom stress term follows the same pattern as observed at 24 m, opposing the wind stress term. The peaks in bottom stress term are lagged with respect to the timing of the wind peaks measured at CSO. The first wind peak (starting 11 March 19:00 UTC) is followed by a maximum bottom stress that occurred 19 h later (12 March 16:00 UTC).

OSD
12, 897–924, 2015

4 Discussion

4.1 Momentum evolution in the inner-shelf

From the estimated momentum terms, we may conclude that the primary balance at 24 m (Fig. 3) takes place between acceleration, wind, bottom friction, advective terms and pressure gradient. Coriolis and radiation stress played secondary roles in the momentum balance.

During the first peak (12 March), as the wind stress term grows, the acceleration term becomes more negative and the bottom stress more positive, as expected from the direction of the flow (Fig. 2a). The peak in the acceleration term occurs before the wind maximum, as a result of the enhanced frictional dissipation and the increase of the pressure gradient force. Thus, the along-shelf current (Fig. 2a) is limited by the intensity of the bottom friction.

During the calm period (13 March), the acceleration term is close to zero until 13 March 10:00 UTC. At that point, the acceleration becomes more negative, likely as the response to an increase in the negative pressure gradient force (expected from the slight decrease in sea level during 13 March, Fig. 2d). The sea level fluctuation may have been a direct response to the change in wind direction or may have been caused by a relaxation following the first wind peak. The along-shelf flow did not reverse (Fig. 2b) and neither did the bottom friction term (Fig. 3f). During the calm period, the advection terms become larger than during the stress-peak period (12 March), suggesting a non-linear response to the forcing.

The second wind peak shares some characteristics with the first one. The acceleration term and the PGFR are enhanced during the increase in wind stress. Before the wind stress starts to decrease, the acceleration exhibits large fluctuations (Fig. 3a) that are also transferred to the bottom friction, Coriolis and PGFR terms. During the second peak of the storm, the advective terms also respond with intense fluctuations in both components. These fluctuations likely are a result of the increased energy available in the system, not properly dissipated by the bottom stress.

OSD
12, 897–924, 2015

The analysis highlights the importance of the initial conditions (whether the system starts from rest or not) and the complexity of the momentum fluctuations during the development of the storm. A comparison of the shifting momentum during both wind peaks shows that the role of the acceleration and advective terms is quite different. During the first peak, the advective terms are relatively small as a result of the linear response of the pressure gradient and bottom stress to the wind forcing. During the second peak, however, the adjustments of the local sea level and the increase in available kinetic energy not dissipated by the bottom friction (still remaining from the first wind peak) result in an increase of the non-linearity of the flow.

The radiation stress terms are one order of magnitude smaller than the primary balance suggested before (i.e. acceleration, pressure gradient and frictional terms). Their sizes are consistent with other studies that neglect the wave forcing over the inner-shelf (outside of the surf zone) because of the lack of wave breaking (Lentz, 1999; Fewings and Lentz, 2010). In a region 150 km north of our area (coastal region offshore of the Tet River), Michaud et al. (2012) confirmed numerically that the wave effects on the inner-shelf circulation are relatively small at 28 m water depth even during a storm event.

4.2 Frictional adjustment and Ekman depth in the inner-shelf

During the first wind peak, the increase in along-shelf velocity led to enhanced bottom stress, until the latter balanced wind stress and along-shelf pressure gradient, therefore achieving a complete frictional adjustment. A measure of the frictional adjustment time can be extracted from the observations, considering the cross-zero momentum and inflexion points in the time series. During the first peak (12 March), the estimates are less uncertain because we can assume than the flow started from rest and the non-linearities were small. The second peak included the local adjustment in sea level and advection, which increases the complexity of the momentum balance. A maximum value for the frictional adjustment time is about 14 h (from 11 March 20:00 UTC to 12 March 10:00 UTC), corresponding to the time between zero and maximum bottom

OSD
12, 897–924, 2015

stress during the first wind pulse. This frictional adjustment time doubles the frictional time as computed from the linear drag law of the bottom stress term ($t = H/r = 7.8$ h) and is consistent with typical values from similar depths. For instance, Winant and Beardsley (1979) provided estimates ranging between 7 and 26 h at depths between 28 and 31 m. During the calm period (13 March), the frictional adjustment cannot be established, because even though there was a decrease in depth-averaged along-shelf velocity (Fig. 2d), the wind duration and magnitude were too small.

To provide a framework for the frictional time, we consider Csanady's (1981) linearized analytical model, applied to the first wind peak period. The along-shelf velocity response to a steady wind stress, considering only bottom friction, is controlled by the following expression:

$$\frac{\partial \overline{v}}{\partial t} = \frac{\tau_{ys}}{\rho H} - \frac{\tau_{yb}}{\rho H}. \tag{7}$$

Solving this equation (see Appendix), we obtain an exponential relation with a characteristic frictional adjustment time scale (t_f).

$$t_f = \frac{H}{2\sqrt{\frac{\tau_{ys} C_{da}}{\rho}}}, \tag{8}$$

where C_{da} is a bottom drag coefficient associated with the depth averaged velocity. For a value of wind stress of 0.12 Pa (averaged value during the first peak), t_f is 13 h. This magnitude agrees fairly well with the frictional adjustment time estimated from observations (about 14 h) and confirms the short response time of the along-shelf current. Therefore, the adjustment time scale expected from a geostrophic balance is larger ($f^{-1} = 18.15$ h) than the frictional time scales in the inner shelf. This result is consistent with the reduced importance of the Coriolis term in the along-shelf momentum balance and highlights the dependence of the flow on bottom dissipation at depths of the order of 24 m during a storm, precluding the appearance of inertial fluctuations independently of the coastal constraint.

OSD
12, 897–924, 2015

The sea surface adjustment time estimated from observations during the storm is of the same order of magnitude as the time scale of the forcing wind. The sea level adjustment is characterized by two separate components: one responding to local wind forcing and another associated with sea level oscillations at scales of the order of the external Rossby radius (Hickey, 1984), or about 100 km in the Catalan Shelf. These large scale fluctuations need a longer time to be compensated.

The short frictional adjustment time is related with the inner-shelf nature of the study site during the storm. The inner-shelf is defined as the region where the combined surface and bottom boundary layers occupy the entire water column (Lentz, 1994). Obviously, the boundaries of the inner-shelf region vary in time depending of the intensity of the forcing mechanism. The bottom and surface Ekman depth can be obtained from empirical formulations such as (Weatherly and Martin, 1978):

$$\delta = \frac{1.3u^*}{\sqrt{Nf}} \tag{9}$$

where $u^* = (\tau_s/\rho)^{1/2}$ is the friction velocity, τ_s is surface/bottom stress magnitude and $N^2 = g\mathrm{d}\rho/\mathrm{d}z$ is the squared buoyancy frequency. The time evolution of the surface and bottom Ekman layers (Fig. 5) is computed iteratively (as N depends on the vertical position within the water column). The buoyancy frequency for Eq. (8) is estimated using the CTD measurements during 17 March (two days after the storm; Grifoll et al., 2012). The N values are estimated to be $0.03\,\mathrm{s}^{-1}$ for the surface layer and $0.005\,\mathrm{s}^{-1}$ for the bottom layer. The boundary layers overlapped most of the time during the storm event (Fig. 5). Even though the applicability of Eq. (8) has been questioned for areas influenced by freshwater discharge (Garvine, 2004; Dzwonkowski et al., 2014), the calculated Ekman layer depths are consistent with the importance of the frictional terms in the along-shelf dynamics. Periods with less energetic wind conditions exhibit smaller wind stress, so the relative importance of the Coriolis term is enhanced at 24 m (Grifoll et al., 2012).

OSD
12, 897–924, 2015

4.3 Cross-shelf variability of the along-shelf momentum terms

The cross-shelf variability of the along-shelf momentum is investigated with the help of the momentum terms calculated at 50 m water depth. The frictional adjustment time, as observed through the evolution of the momentum terms at 50 m, exhibited a 4 h lag when compared with the frictional adjustment time at 24 m (Sect. 4.1), likely caused by the time delay in the vertical transfer of momentum. The resulting linear drag coefficient, $r = 7.3 \times 10^{-4}\,\mathrm{m\,s^{-1}}$, is close to the r value for the inner-shelf ($8.5 \times 10^{-4}\,\mathrm{m\,s^{-1}}$), supporting our analysis during the first storm peak, in terms of the linear response to wind stress and the pressure gradient estimated from the residual.

The relative ratio of the fluctuations (Standard Deviations: SDs) in the acceleration and wind stress terms, ($\frac{\rho_0 H \partial \overline{v}/\partial t}{\tau_{ys}}$), increases offshore (from 1.10 at 24 m to 1.36 at 50 m). These values are larger than estimates from other shelves (Lentz and Fewings, 2012): in the Middle Atlantic Bight, around 0.3 and 0.5 at 25 and 50 m, respectively; and in the West Florida Shelf, 0.5 and 1 for 25 and 50 m, respectively. The larger values found in the Catalan Shelf are ascribed to the enhanced acceleration during the storm.

The size of the Coriolis term at 50 m increases in comparison to the size of this term estimated at 24 m water depth. The SD also increases offshore, from $9.6 \times 10^{-7}\,\mathrm{m\,s^{-2}}$ at 24 m to $1.5 \times 10^{-6}\,\mathrm{m\,s^{-2}}$ at 50 m. The ratio of the fluctuations between the Coriolis and wind stress terms $\frac{\rho_0 H f \overline{u}}{\tau_{ys}}$ increased from 0.3 at 24 m to 1.3 at 50 m water depth. Lentz and Fewings (2012) presented ratios around 0.4 for the Middle Atlantic Bight and West Florida Shelf at 25 m, and between 2 and 3 at 50 m depth.

The increasing/decreasing importance of the Coriolis/bottom-frictional terms responds to a switch towards the geostrophic balance, typical in the transition from the inner to the mid-shelf. With increasing depth, the frictional effects decrease in the along-shelf momentum balance. Lee et al. (1984) observed that the Coriolis term doubled from 28 to 75 m water depth in the South Atlantic Bight (USA), with progressively smaller frictional terms. At the start of our study period (11 March 2011; see

OSD
12, 897–924, 2015

Fig. 4), the 50 m water depth Coriolis term was larger than the other terms, suggesting a geostrophic balance during the calm period.

During the storm period, the $PGFR_{ACCE+COR+FRIC}$ term (at 50 m) is moderately correlated with the Coriolis term ($R = 0.55$ with 95 % confidence level). This correlation suggests that the dynamic response at 50 m includes a significant geostrophic component, in contrast to the balance at 24 m where the PGFR were not as correlated with Coriolis ($R = 0.33$ with 95 % confidence level). However, the acceleration and frictional terms, and likely the non-linear terms, also played an important role at 50 m water depth during the storm; for example, the acceleration terms at 24 and 50 m are also moderately correlated ($R = 0.64$ with 95 % confidence level). Michaud et al. (2013), from observations in the Gulf of Lion (275 km north of our study area; see Fig. 1) at 65 m depth, also emphasized the importance of the wind-induced geostrophic currents during a storm.

The cross-shelf changes in the relative importance of the frictional and geostrophic terms in the along-shelf momentum balance (Fig. 6) can be explored by comparing the frictional times (Eq. 7) with the inertial time ($f^{-1} = 18.15$ h). The frictional and inertial times during the peak of the storm (surface stress $\tau = 0.25$ Pa) are equal for water depths of 94 m; for the average stress of the storm (surface stress $\tau = 0.12$ Pa) this happens for water depths of 64 m. Thus, the frictional effects dominated for depths up to around 60 m, causing our current meters to be located in regions controlled by inner-shelf dynamics during the whole storm. For the frictional and inertial times to be the same the wind stress would have to be 0.075 Pa at 50 m and 0.02 Pa at 24 m. Therefore, the Coriolis term of the momentum balance is not important at 24 m except for very low surface stresses, such as during the calm period between the two storm pulses (0.02 Pa); during those times other terms, like the pressure gradient force, will dominate the along-shelf momentum balance (Grifoll et al., 2013).

OSD
12, 897–924, 2015

5 Conclusions and final remarks

Our analysis has assessed the effects of the passage of a storm over the inner Catalan Shelf (NW Mediterranean Sea) on the along-shelf momentum balance. At 24 m water depth, a primary momentum balance between the acceleration, pressure gradient and frictional (surface and bottom) terms was established. The advection terms apparently were occasionally important, but difficult to estimate from observations. The Coriolis and the wave-induced momentum terms play a second order role in the momentum balance. The storm had two separate peaks that caused distinct responses: during the first peak the advective terms were small (i.e. linear response) but during the second peak they increased markedly; this non-linear behavior happened via a local adjustment to pressure gradient, as a result of the increased kinetic energy from the initial wind peak that the bottom stress was not able to dissipate. The frictional adjustment time and Ekman depth estimates confirmed the prevalence of the frictional response of the flow at 24 m. The increasing importance of Coriolis at 50 m corresponds to a shift towards the geostrophic behavior, characterizing the transition from the inner to the mid-shelf.

In our analysis, we have focused on the shelf response to a single storm, where extensive observational data were available. However, northeasterly energetic wind events are common during spring and fall in the Catalan Shelf, so similar events are expected on a yearly basis. The extrapolation of our results to other shelves depends on physical variables such as stratification, river discharge and remote sea-level forcing. In relatively low-energy shelves, such as the Catalan shelf, it is plausible that two-peak storms be commonly characterized by a sequence of linear response followed by a subsequent non-linear behavior.

Early investigations (e.g. Scott and Csanady, 1976) pointed out that tidally driven fluctuations difficult the analysis of the wind induced circulation at depths where the frictional adjustment time is similar to tidal periods. For this reason, in tidal active regions, wind-driven changes at scales shorter than the semidiurnal period are very dif-

OSD
12, 897–924, 2015

ficult to detect; the associated depth for this period is about 60 m in typical wind events (Csanady, 1981). In contrast, the micro-tidal nature of Catalan shelf has allowed us to investigate in detail the shelf response at temporal scales shorter than previously investigated for the inner-shelf.

Appendix: Frictional adjustment time for linear and quadratic formulations

A simple model to determine the frictional time adjustment was presented by Csanady (1981), based on the transport momentum equation in the along-shelf direction:

$$\frac{\partial V}{\partial t} + fU = -gH\frac{\partial \eta}{\partial y} + u^{*2} - \frac{\tau_{yb}}{\rho}, \tag{A1}$$

where the transport is:

$$U = \int_{-H}^{0} u\mathrm{d}z, \tag{A2a}$$

$$V = \int_{-H}^{0} v\mathrm{d}z, \tag{A2b}$$

and the frictional velocity is given by:

$$u^* = \sqrt{\frac{\tau_{ys}}{\rho}}. \tag{A3}$$

Under the assumption that the depth distribution is only a function of the cross-shelf coordinate, we neglect the along-shelf pressure gradients. If the depth distribution is taken only in function of x so there is no reason why pressure gradients should emerge. Also,

OSD
12, 897–924, 2015

the coastal constraint near the coast implies $U = 0$. These conditions lead a frictional balance between the acceleration and the wind and bottom stresses:

$$\frac{\partial V}{\partial t} = u^{*2} - \frac{\tau_{yb}}{\rho}. \tag{A4}$$

The bottom stress was parameterized by Csanady (1981) using a quadratic drag law equation in function of the depth-averaged current (V/H):

$$\frac{\tau_{yb}}{\rho} = C_{da}\left(\frac{V}{H}\right)^2. \tag{A5}$$

Integrating, the solution for the along-shelf transport follows an exponential equation:

$$V = \frac{u^* H}{\sqrt{C_{da}}}\left(\frac{1 - \exp\left(-2u^* t\sqrt{C_{da}}/H\right)}{1 + \exp\left(-2u^* t\sqrt{C_{da}}/H\right)}\right), \tag{A6}$$

with an e-folding time scale of:

$$t_f = \frac{H}{2\sqrt{\frac{\tau_{ys}\cdot C_{da}}{\rho}}}. \tag{A7}$$

Alternatively, we may consider the bottom frictional term to depend linearly on the depth-averaged current:

$$\frac{\tau_{yb}}{\rho} = r\left(\frac{V}{H}\right). \tag{A8}$$

In this case, the solution follows again an exponential solution:

$$V = \frac{u^{*2} H}{r}\left(1 - \exp^{-\frac{r}{H}t}\right), \tag{A9}$$

OSD
12, 897–924, 2015

where the e-folding time scale is H/r, as expected according to the lineal parametrization of the bottom stress in Eq. (2). Linear and quadratic derived frictional time expressions have the same physical meaning, with e-folding times proportional to the water depth and inversely proportional to bottom stress parameter (e.g. r o C_{da}). For the linear and quadratic formulations, at long times the depth-averaged velocities tend asymptotically to $\frac{u^*}{\sqrt{C_{da}}}$ and $\frac{u^{*2}}{r}$, respectively, which are the velocities required for bottom stress to balance the wind stress.

Acknowledgements. This work was supported by DARDO (ENE2012-38772-C02-02) and ICoast project (Echo/SUB/2013/661009). We would like to thank Joan Puigdefàbregas, Jordi Cateura and Joaquim Sospedra (LIM-UPC, Barcelona, Spain) for the data acquisition campaign.

References

Booij, N., Ris, R. C., and Holthuijsen, L. H.: A third-generation wave model for coastal regions: 1. Model description and validation, J. Geophys. Res., 104, 7649, doi:10.1029/98JC02622, 1999.

Csanady, G. T.: Circulation in the coastal ocean, Adv. Geophys., 23, 101–183, 1981.

Dzwonkowski, B., Park, K., Lee, J., Webb, B. M., and Valle-Levinson, A.: Spatial variability of flow over a river-influenced inner shelf in coastal Alabama during spring, Cont. Shelf Res., 74, 25–34, doi:10.1016/j.csr.2013.12.005, 2014.

Fewings, M. R. and Lentz, S. J.: Momentum balances on the inner continental shelf at Martha's Vineyard Coastal Observatory, J. Geophys. Res., 115, C12023, doi:10.1029/2009JC005578, 2010.

Garvine, R. W.: The vertical structure and subtidal dynamics of the inner shelf off New Jersey, J. Mar. Res., 62, 337–371, doi:10.1357/0022240041446182, 2004.

Grifoll, M., Aretxabaleta, A. L., Espino, M., and Warner, J. C.: Along-shelf current variability on the Catalan inner-shelf (NW Mediterranean), J. Geophys. Res., 117, 1–14, doi:10.1029/2012JC008182, 2012.

OSD
12, 897–924, 2015

Grifoll, M., Aretxabaleta, A. L., Pelegrí, J. L., Espino, M., Warner, J. C., and Sánchez-Arcilla, A.: Seasonal circulation over the Catalan inner-shelf (northwest Mediterranean Sea), J. Geophys. Res.-Oceans, 118, 5844–5857, doi:10.1002/jgrc.20403, 2013.

Grifoll, M., Gracia, V., Aretxabaleta, A. L., Guillén, J., Espino, M., and Warner, J. C.: Formation of fine sediment deposit from a flash flood river in the Mediterranean Sea, J. Geophys. Res.-Oceans, 119, 5837–5853, doi:10.1002/2014JC010187, 2014.

Hickey, B. M.: The fluctuating longshore pressure gradient on the Pacific Northwest Shelf: a dynamical analysis, J. Phys. Oceanogr., 14, 276–293, doi:10.1175/1520-0485, 1984.

Kirincich, A. R. and Barth, J. A.: Alongshelf Variability of Inner-shelf Circulation along the Central Oregon Coast, J. Phys. Oceanogr., 39, 1380–1398, doi:10.1175/2008JPO3760.1, 2009.

Kohut, J. T., Glenn, S. M., and Paduan, J. D.: Inner shelf response to tropical storm Floyd, J. Geophys. Res., 111, C09S91, doi:10.1029/2003JC002173, 2006.

Large, W. G. and Pond, S.: Open ocean momentum flux measurements in moderate to strong winds, J. Phys. Oceanogr., 11, 324–336, doi:10.1175/1520-0485, 1981.

Lee, T. N., Ho, W. J., Kourafalou, V., and Wang, J. D.: Circulation on the continental shelf of the southeastern United States. Part I: Subtidal response to wind and gulf stream forcing during winter, J. Phys. Oceanogr., 14, 1001–1012, doi:10.1175/1520-0485, 1984.

Lentz, S.: Current dynamics over the Northern California Inner Shelf, J. Phys. Oceanogr., 24, 2461–2478, 1994.

Lentz, S., Guza, R. T., Elgar, S., Feddersen, F., and Herbers, T. H. C.: Momentum balances on the North Carolina Inner Shelf, J. Geophys. Res., 104, 18205–18226, doi:10.1029/1999JC900101, 1999.

Lentz, S. J. and Fewings, M. R.: The wind- and wave-driven inner-shelf circulation, Ann. Rev. Mar. Sci., 4, 317–343, doi:10.1146/annurev-marine-120709-142745, 2012.

Lentz, S. J. and Winant, C. D.: Subinertial currents on the Southern California Shelf, J. Phys. Oceanogr., 16, 1737–1750, doi:10.1175/1520-0485, 1986.

Longuet-Higgins, M. and Stewart, R.: Radiation stresses in water waves; a physical discussion, with applications, Deep-Sea Res. Pt. II, 11, 529–562, 1964.

Maza, M., Voulgaris, G., and Subrahmanyam, B.: Subtidal inner shelf currents off Cartagena de Indias, Caribbean coast of Colombia, Geophys. Res. Lett., 33, 1–5, doi:10.1029/2006GL027324, 2006.

OSD
12, 897–924, 2015

Michaud, H., Marsaleix, P., Leredde, Y., Estournel, C., Bourrin, F., Lyard, F., Mayet, C., and Ardhuin, F.: Three-dimensional modelling of wave-induced current from the surf zone to the inner shelf, Ocean Sci., 8, 657–681, doi:10.5194/os-8-657-2012, 2012.

Michaud, H., Leredde, Y., Estournel, C., Berthebaud, É., and Marsaleix, P.: Modelling and in-situ measurements of intense currents during a winter storm in the Gulf of Aigues–Mortes (NW Mediterranean Sea), C.R. Geosci., 345, 361–372, doi:10.1016/j.crte.2013.07.001, 2013.

Salat, J., Tintore, J., Font, J., Wang, D.-P., and Vieira, M.: Near-inertial motion on the shelf-slope front off northeast Spain, J. Geophys. Res., 97, 7277–7281, doi:10.1029/92JC00588, 1992.

Scott, J. T. and Csanady, G. T.: Nearshore currents off Long Island, J. Geophys. Res., 81, 5401–5409.

Shearman, R. K.: Observations of near-inertial current variability on the New England Shelf, J. Geophys. Res., 110, C02012, doi:10.1029/2004JC002341, 2005.

Weatherly, G. and Martin, P.: On the structure and dynamics of the oceanic bottom boundary layer, J. Phys. Oceanogr., 8, 557–570, 1978.

Winant, C. D. and Beardsley, R. C.: A comparison of some shallow wind-driven currents, J. Phys. Oceanogr., 9, 218–220, doi:10.1175/1520-0485(1979)009<0218:ACOSSW>2.0.CO;2, 1979.

OSD
12, 897–924, 2015

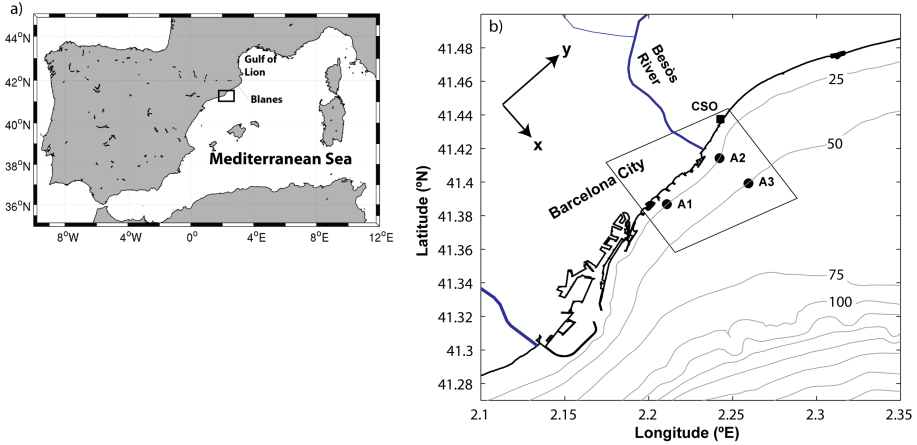

Figure 1. Map of the Western Mediterranean Sea with the study area **(a)**. **(b)** shows the bathymetry of a portion of the Catalan Shelf (isobaths every 25 m) with the locations of the ADCP sensors (A1, A2 and A3). The square marker shows the Coastal Station Observatory (CSO) where the wind data were recorded. **(b)** includes the numerical model domain used to propagate the wave conditions into A2 (black rectangle); the reference system adopted for the momentum balance is shown.

OSD
12, 897–924, 2015

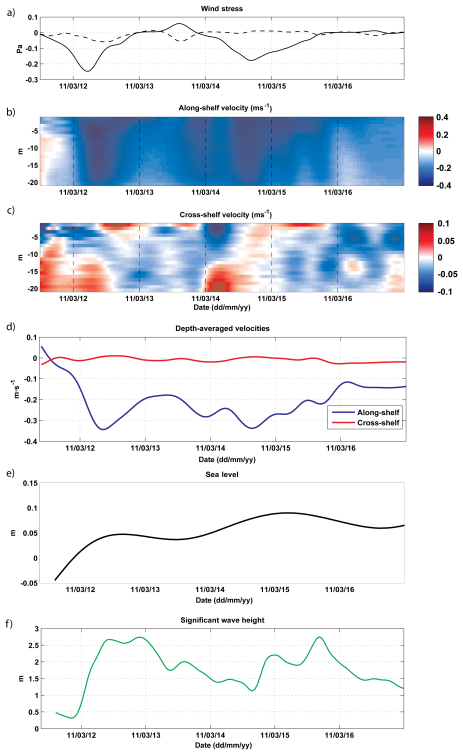

Figure 2. (a) Time series of wind stress measured at the Coastal Observatory Station (the continuous line for the along-shelf wind component and the dashed line for the cross-shelf wind component). **(b)** Along-shelf velocity. **(c)** Cross-shelf velocity. **(d)** Depth-averaged along- and cross-shelf velocities. **(e)** Detided sea-level variations. **(f)** Significant wave-height. The velocities and sea level fluctuations were measured at station A2, and the wave conditions at station A3. The date indicates 00:00 UTC.

OSD
12, 897–924, 2015

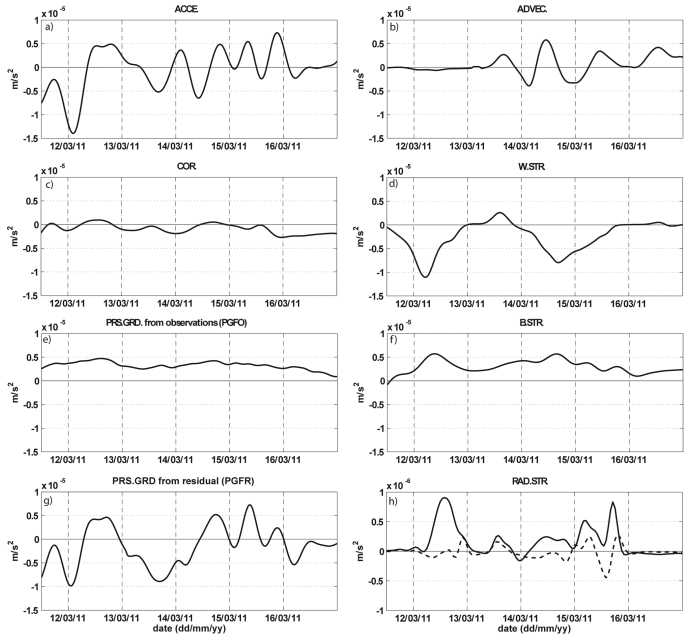

Figure 3. Estimates for the along-shelf momentum terms at 25 m. Left-hand-side terms of Eq. (1): **(a)** acceleration terms (ACCE $\delta v/\delta t$); **(b)** advective non-linear terms (ADVEC $\delta v^2/\delta y + \delta(vu)/\delta x$) estimated differentiating between the currents at the neighboring ADCP locations; **(c)** Coriolis (COR fu). Right-hand-side terms of Eq. (1): **(d)** wind stress term (W-STR $\tau_{ys}/\rho H$); **(e)** pressure gradient force from observations (PGFO term; $-g\delta\eta/\delta y$); **(f)** bottom stress term (B-STR $-\tau_{yb}/\rho H$); **(g)** pressure gradient force from residual (PGFR); **(h)** radiation stress term (RAD-STR $-(1/\rho H)\delta S_{xy}/\delta x$ continuous line and $-(1/\rho H)\delta S_{yy}/\delta y$ dashed line). Note that the change in the vertical scale in **(h)**. The data used for estimating the momentum terms have been low-pass filtered, with a cut-off frequency of 12 h^{-1}. The date indicates 00:00 UTC.

OSD
12, 897–924, 2015

Shifting momentum balance and frictional adjustment observed over the inner-shelf during a storm

M. Grifoll et al.

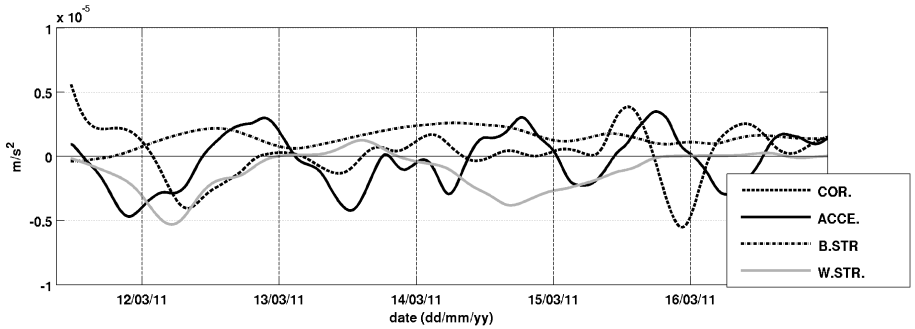

Figure 4. Estimates for the along-shelf momentum terms at 50 m. Left-hand-side terms of Eq. (1): acceleration terms (ACCE $\delta v/\delta t$) and Coriolis (COR fu). Right-hand-side terms of Eq. (1): wind stress term (W-STR $\tau_{ys}/\rho H$) and bottom stress term (B-STR $-\tau_{yb}/\rho H$). The data used for estimating the momentum terms have been low-pass filtered with a cut-off frequency of 12 h^{-1}. The date indicates 00:00 UTC.

OSD
12, 897–924, 2015

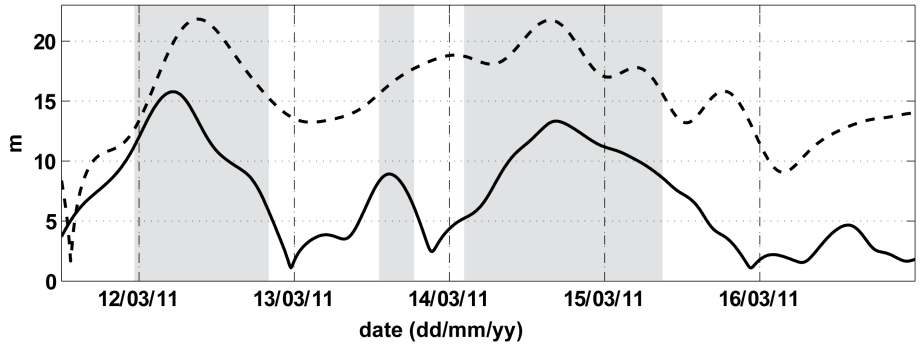

Figure 5. Estimates of the surface (continuous line) and bottom (dashed line) Ekman depths (in m). The gray patch shows the periods where the sum of the surface and bottom Ekman depths exceeded 24 m (the water depth at station A2). The date indicates 00:00 UTC.

OSD
12, 897–924, 2015

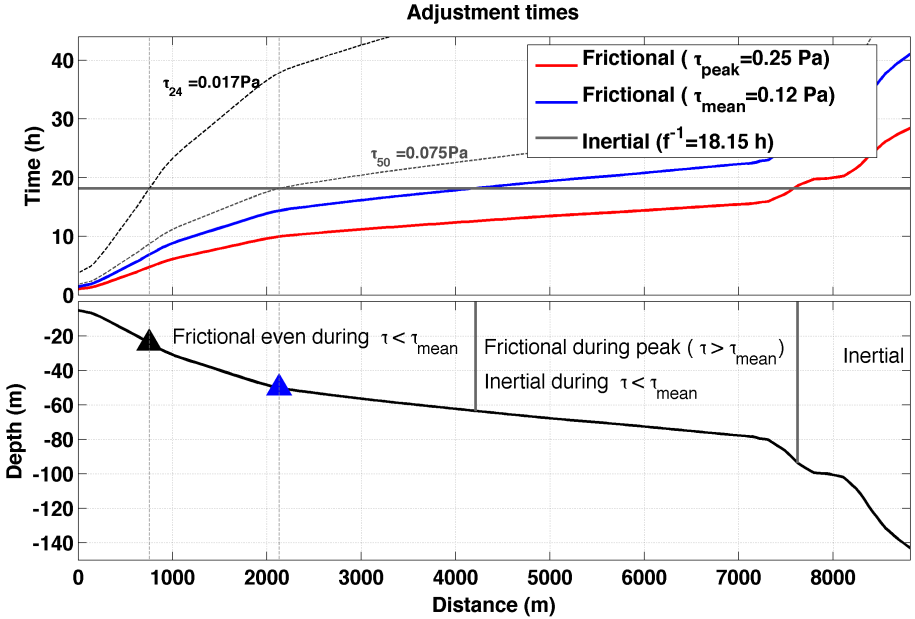

Figure 6. Top panel: cross-shelf transect of the frictional adjustment times for several wind stresses together with the inertial time off the city of Barcelona (18.15 h, grey solid line). The cross-shelf variation of the frictional adjustment time (computed following Eq. 7) is shown for storm peak conditions (red line) and averaged storm conditions (blue line). The two dotted lines correspond to wind stresses such that the frictional and inertial times become equal at 24 m (t_{24}) and 50 m (t_{50}) water depth. Bottom panel: the location of the inertial, frictional and transition zones for the peak and mean storm conditions. The ADCP locations at 24 and 50 m are indicated with black and blue triangles, respectively.

OSD
12, 897–924, 2015